# Self-diffusion in fluids in microporous solids

T. K. Vanderlick and H. T. Davis
*Department of Chemical Engineering and Materials Science, University of Minnesota, Minneapolis, Minnesota 55455*

(Received 15 December 1986; accepted 26 February 1987)

Enskog's kinetic theory of tracer diffusion has been generalized recently to strongly inhomogeneous fluids and is here applied to self-diffusion in fluids in slit pores, i.e., fluids confined between parallel, flat, solid walls. In pores narrower than ten molecular diameters, the diffusivity deviates significantly from its value in bulk phase at the same temperature and chemical potential. Because of the confining pore walls, the fluid tends to form layers. The pore diffusivity oscillates as a function of pore width, a local minimum occurring when the packing of a given number of fluid layers is favored and a local maximum in the region of transition between these favored packing widths. The theory predicts fluid density distributions in good agreement with computer simulations of a similar fluid. The predicted diffusivities are in good qualitative agreement with computer simulations, although quantitatively the predicted oscillations are sharper than those observed in the computer simulations. This work represents the first application of Enskog's kinetic theory of diffusion in strongly inhomogeneous fluids.

## I. INTRODUCTION

Practical instances of fluid transport in microporous media abound, e.g., separations or catalytic processes in zeolites, reverse osmosis membrane separations, solvent swelling rubbers, polyelectrolyte gels, and gas permeation of Vicor glass. In spite of this, a tractable molecular theory of transport of fluids in micropores has not been developed. As a first step towards achieving such a theory, one of us (HTD) recently generalized Enskog's theory of tracer diffusion in homogeneous fluid to the case of tracer diffusion in strongly inhomogeneous fluids.[1] The purpose of this paper is to apply the theory to self-diffusion in fluids confined between flat, solid surfaces, i.e., fluids in a slit pore. Two model fluids, a hard sphere fluid and a Lennard-Jones fluid are examined. The theoretical results for the density and pore diffusivity are compared to available computer simulations on a similar Lennard-Jones fluid.[2,3]

## II. KINETIC THEORY

Enskog's kinetic theory has been generalized recently to tracer diffusion in strongly inhomogeneous fluids. The local diffusion flux is predicted to be of the form[1]

$$\mathbf{J}_1 = -n_1^0 k_B T \boldsymbol{\zeta}^{-1} \cdot \nabla (n_1/n_1^0) , \tag{1}$$

where $\nabla$ is the gradient operator, $k_B$ Boltzmann's constant, $T$ the temperature, $n_1^0$ the equilibrium density distribution, $n_1$ the density distribution under the transport conditions, and $\boldsymbol{\zeta}$ the friction tensor. The friction tensor at position $\mathbf{r}$ is given by

$$\boldsymbol{\zeta}(\mathbf{r}) = \sum_{j \neq 1} \frac{m_1}{\pi} \left( \frac{2\pi k_B T}{m_{1j}} \right)^{1/2} \times \int g_{1j}(\mathbf{r}, \mathbf{r} + \sigma_{1j}\mathbf{k}) n_j^0 (\mathbf{r} + \sigma_{1j}\mathbf{k}) \sigma_{1j}^2 \mathbf{k}\mathbf{k}\, d^2k , \tag{2}$$

where $m_j$ is molecular mass, $m_{1j} = m_1 m_j/(m_1 + m_j)$, $g_{1j}(\mathbf{r},\mathbf{r}')$ the pair correlation function between a pair of particles of species 1 and $j$, $n_j^0(\mathbf{r})$ the equilibrium density distribution of species $j$ at position $\mathbf{r}$, $\sigma_j$ the hard sphere diameter of species $j$, $\sigma_{1j} \equiv (\sigma_1 + \sigma_j)/2$, $\mathbf{k}$ a unit vector between particles 1 and $j$, and $d^2k$ the element of solid angle. It follows from Eqs. (1) and (2) that the friction tensor and, therefore, the diffusion tensor, are anisotropic in an inhomogeneous fluid.

The equilibrium density distribution $n_1^0$ obeys the Yvon–Born–Green (YBG) equation

$$k_B T \nabla n_i^0 + n_i \nabla u_i^e - n_i^0 \sum_j \int n_j^0(\mathbf{r} + \mathbf{s}) g_{ij}(\mathbf{r}, \mathbf{r} + \mathbf{s}) \times \frac{\mathbf{s}}{s} \frac{du_{ij}^A}{ds} d^3s + n_i^0 \sum_j k_B T \int g_{ij}(\mathbf{r}, \mathbf{r} + \sigma_{ij}\mathbf{k}) \times n_j^0(\mathbf{r} + \sigma_{ij}\mathbf{k}) \sigma_{ij}^2 \mathbf{k}\, d^2k = 0 . \tag{3}$$

$u_{ij}^A$ is the attractive part of the pair interaction potential. In the model, it is assumed that the molecular forces are pair additive and that the pair potential consists of a sum of a continuous nondissipative part, $u_{ij}^A$, and a hard sphere part whose dissipative interactions are accounted for in the uncorrelated binary collision approximation. The quantity $u_i^e$ denotes the external potential energy, including the interaction between fluid particles and solid surfaces.

To render Eq. (3) solvable, one must introduce an approximation relating $g_{ij}$ to fluid density distributions. We choose here the rather successful one introduced by Fischer and co-workers.[4,5] According to their approximation, the contact value of the correlation function is given by

$$g_{ij}(\mathbf{r}, \mathbf{r} + \sigma_{ij}\mathbf{k}) = g_{ij}^{\mathrm{HS}} [r_{ij} = \sigma_{ij}; \bar{\mathbf{n}}(\mathbf{r} + \tfrac{1}{2}\sigma_{ij}\mathbf{k})] , \tag{4}$$

where $g_{ij}^{\mathrm{HS}}$ is the contact value of the pair correlation function of hard spheres in a homogeneous fluid in the average local density state $\bar{\mathbf{n}}(\mathbf{r} + \frac{1}{2}\sigma_{ij}\mathbf{k})$. $\mathbf{n}$ denotes the component density set $\{n_1, n_2, \ldots\}$. The local average densities are defined by

$$\bar{n}_i(\mathbf{r} + \tfrac{1}{2}\sigma_{ij}\mathbf{k}) = \frac{1}{\pi\sigma_{ij}^3/6} \int_{R < \sigma_{ij}/2} n_i(\mathbf{r} + \tfrac{1}{2}\sigma_{ij}\mathbf{k} + \mathbf{R}) d^3R . \tag{5}$$

 0021-9606/87/151791-05$02.10  

Fischer and co-workers assume further that the structureless fluid approximation, $g_{ij} = 1$, can be used in evaluating the integral involving the nondissipative forces $du_{ij}^A/ds$.

In what follows we examine the case of self-diffusion in a one component fluid confined by two flat, impermeable, solid walls, i.e., fluid in a slit pore. By self-diffusion, we mean that the molecular properties of the tracer particles are identical with those of the other fluid particles. The particle-well potential $u^e$ is assumed to be a function only of the distance $x$ of the particle from the wall. The equilibrium density distributions $n_i^0$ in the slit pore depend only on the distance $x$ from the wall. If $n_i^0$ denotes the tracer particle density and $n^0$ the density of the other fluid particles, then the YBG equations to be investigated in this paper are

$$k_BT\frac{dn_1^0}{dx}+n_1^0\frac{du^e}{dx}-n_1^0\int n^0(x+s_x)\frac{s_x}{s}\frac{du^A}{ds}(s)d^3s + 2\pi\sigma^2 n_1^0 k_BT\int_{-1}^{1} g^{HS}[\sigma;\bar{n}^0(x+\tfrac{1}{2}\sigma\xi)] \times n^0(x+\sigma\xi)\xi d\xi = 0, \tag{6a}$$

$$k_BT\frac{dn^0}{dx}+n^0\frac{du^e}{dx}-n^0\int n^0(x+s_x)\frac{s_x}{s}\frac{du^A}{ds}(s)d^3s + 2\pi\sigma^2 n^0 k_BT\int_{-1}^{1} g^{HS}[\sigma;\bar{n}^0(x+\tfrac{1}{2}\sigma\xi)] \times n^0(x+\sigma\xi)\xi\, d\xi = 0. \tag{6b}$$

In tracer diffusion the density $n_1$ of the tracer particles is negligible compared to the solvent density $n$. Accordingly, we have neglected in Eq. (6a) terms of order $n_1^2$ and in Eq. (6b) we have ignored terms of order $n_1$.

For the hard sphere correlation junction $g^{HS}$ we use the following formula, which Carnahan and Starling have shown to be accurate for hard sphere fluids[6]:

$$g^{HS}(\sigma;\bar{n}) = \left(1-\frac{\pi}{12}\bar{n}\sigma^3\right)\Big/\left(1-\frac{\pi}{6}\bar{n}\sigma^3\right)^3. \tag{7}$$

We note that it is only necessary to solve Eq. (6b) for the fluid density $n^0$. It follows from Eqs. (6a) and (6b) that

$$\frac{d\ln[n_1^0]}{dx}=\frac{d\ln[n^0]}{dx}$$

and so $n_1^0/n^0 =$ constant. Thus, the equilibrium tracer and solvent density distributions are related by a constant scale factor set by the ratio of the total numbers of tracer and solvent particles.

## III. SELF-DIFFUSION IN A SLIT PORE

For the slit pore the friction tensor is of the form

$$\zeta = \zeta_N\hat{n}\hat{n} + \zeta_T(\hat{i}\hat{i}+\hat{k}\hat{k}), \tag{8}$$

where $\hat{i}, \hat{j}$, and $\hat{k}$ are unit vectors in the $x$, $y$, and $z$ directions and the normal and transverse components of the friction tensor are given by

$$\xi_N(x) = 4\sigma^2(\pi m k_BT)^{1/2}\int_{-1}^{1} g^{HS}[\sigma;\bar{n}^0(x+\tfrac{1}{2}\sigma\xi)] \times n^0(x+\sigma\xi)\xi^2 d\xi \tag{9}$$

and

$$\zeta_T(x) = 4\sigma^2(\pi m k_BT)^{1/2}\int_{-1}^{1} g^{HS}[\sigma;\bar{n}^0(x+\tfrac{1}{2}\sigma\xi)] \times n^0(x+\sigma\xi)(1-\xi^2)d\xi. \tag{10}$$

The diffusion flux corresponding to Eq. (8) is

$$\mathbf{J}_1 = -n_1^0 D_N\hat{i}\frac{\partial}{\partial x}\ln(n_1/n_1^0) - D_T\left[\hat{j}\frac{\partial n_1}{\partial y}+\hat{k}\frac{\partial n_1}{\partial z}\right], \tag{11}$$

where $D_N \equiv k_BT/\zeta_N$ and $D_T \equiv k_BT/\zeta_T$. Pore wall impermeability yields the condition $J_{1x} = 0$. We choose $y$ to be the diffusion direction so that $J_{1z} = 0$. These conditions imply that $n_1$ is independent of $z$ and $n_1(x,y) = n_1^0(x)\chi(y)$. Thus,

$$J_{1y} = -D_T(x)n_1^0(x)\frac{d\chi(y)}{dy}. \tag{12}$$

Experimentally one would not expect to measure the local flux but rather the pore average flux $J_{pore}$ and pore average density $n_{pore}$ defined by

$$J_{pore} = \frac{1}{h}\int_0^h J_{1y}\,dx \quad\text{and}\quad n_{pore} = \frac{1}{h}\int_0^h n_1\,dx, \tag{13}$$

where $h$ is the distance of separation of the pore walls. From these definitions and Eq. (12) it follows that

$$J_{pore} = -D_{pore}\frac{dn_{pore}}{dy}, \quad D_{pore} \equiv \frac{\int_0^h D_T(x)n^0(x)dx}{\int_0^h n^0(x)dx}. \tag{14}$$

The pore diffusivity defined by Eq. (14) is the appropriate quantity to compare with the diffusivity obtained in the computer simulations of Magda *et al.*[3] Comparisons will be made in a subsequent section.

## IV. MODEL INPUTS AND THE COMPUTATIONAL METHOD

By integration, we convert Eq. (6b) to the integral equation

$$k_BT\ln n^0(x) = \mu^* - u^e(x) - \int_{-\infty}^{+\infty} n^0(x')\bar{u}^A(|x-x'|)dx' - 2\pi k_BT\sigma^2\int_0^x dx'\int_{-1}^{1} d\xi\,\xi n^0(x'+\sigma\xi) \times g^{HS}\left[\bar{n}\left(x'+\frac{1}{2}\sigma\xi\right)\right], \tag{15}$$

where

$$\bar{n}(x) = (6/\sigma^3)\int_{-\sigma/2}^{+\sigma/2}[0.25\sigma^2-(x-x')^2]n(x')dx'. \tag{16}$$

The parameter $\mu^*$ is a constant of integration which plays the role of a chemical potential.

The external potential $u_e$ arises from the solid walls at $x = 0$, and $x = h$:

$$u^e(x) = \phi_{wall}(x) + \phi_{wall}(h-x),$$

where each wall exerts a 10–4–3 potential:

$$\phi_{\text{wall}}(x) = 2\pi\epsilon_w \left[ \frac{2}{5}\left(\frac{\sigma}{x}\right)^{10} - \left(\frac{\sigma}{x}\right)^4 - \frac{\sqrt{2}\sigma^3}{3\left(x+\frac{0.61\sigma}{\sqrt{2}}\right)^3} \right], \quad x>0$$
$$= \infty, \quad x<0. \tag{17}$$

This implies that $n^0(x) = 0$ for $x<0$, $x>h$. The intermolecular potential,

$$\bar{u}_A(s_x) \equiv \int_{-\infty}^{\infty}\int u^A(s)\,ds_y\,ds_z \tag{18}$$

is chosen to be

$$\bar{u}_A(s_x) = -2\pi\epsilon\sigma^2, \quad |s_x|<\sigma,$$
$$= -\frac{2\pi\epsilon\sigma^6}{|s_x|^4}, \quad |s_x|>\sigma. \tag{19}$$

This corresponds to the attractive pair potential $u^A(s) = 0$, $s<\sigma$, and $u^A(s) = -4\epsilon(\sigma/s)^6$, $s>\sigma$.

In solving Eqs. (15) and (16) we substitute for $n(x)$ the variable $Y(x)$ where

$$Y(x) = n(x)e^{u^e(x)/k_BT}, \tag{20}$$

since this is a more slowly varying function of $x$ in the interval $0<x<h$. The domain of interest, $0<x<h$, is discretized uniformly and the trapezoidal rule is used to evaluate the integrals. Equations (15) and (16) become a system of nonlinear, coupled, algebraic equations for the nodal values of $Y$ and $\bar{n}$. Newton's method is used to solve for $Y$ and $\bar{n}$ simultaneously. The domain is discretized finely enough so that the solution changes negligibly with further refinement. A mesh size of $0.05\sigma$ was used in the calculations reported here.

Solutions were obtained initially for a wall separation $h = 20\sigma$, where at the midpoint the density is equal to the bulk fluid density $n_b$. Then solutions for decreasing pore width were found using the previous solution at larger $h$ as a first guess for the next width. Pore width was gradually decreased to $h = 2.25\sigma$ using small enough steps so that quadratic convergence was observed at each new pore width (steps of size 0.05 were used to track the solution).

## V. RESULTS AND DISCUSSION

The units used for the quantities discussed in this section are given in Table I. We examine two cases: (1) $\epsilon = 0$, a "hard sphere fluid" and (2) $\epsilon = 0.826\,45$, a "6-$\infty$ Lennard-Jones fluid." In both cases the wall–fluid particle interaction potential is given by Eq. (17) with $\epsilon_w = 0.826\,45$. The chemical potential parameter $\mu^*$ is selected so that in the bulk fluid limit ($h = \infty$) the density is $n_b = 0.5925$. For the hard sphere fluid $\mu^* = 4.532$ and for the Lennard-Jones fluid $\mu^* = -3.6265$. The values of $\epsilon$, $\epsilon_w$, and $n_b$ were chosen so that the fluids studied here correspond roughly to be 6–12 Lennard-Jones fluid studied by molecular dynamics by Magda *et al.*[3] and Snook and van Megen.[2]

TABLE I. Units of relevant quantities.

| Quantity | Units |
|---|---|
| Distance | $\sigma$ |
| Wall separation | $\sigma$ |
| Density | $\sigma^{-3}$ |
| Particle–wall energy $\epsilon_w$ | $kT$ |
| Particle–particle energy $\epsilon$ | $kT$ |
| Chemical potential parameter $\mu^*$ | $kT$ |
| Diffusion coefficient | $(3\sigma/8)(kT/\pi m)^{1/2}$ |

In Fig. 1 our predicted density profiles for the hard sphere fluid and the 6-$\infty$ Lennard-Jones fluid in a pore of width 4 are compared with computer simulations for a 6-12 Lennard-Jones fluid. The wall–fluid particle interaction potential is the same as that used in the computer simulations. The Lennard-Jones interactions between fluid particles differs somewhat. The repulsive force in our model is the hard sphere interaction, whereas in the simulations repulsion is given by the inverse 12th power law. Also, in the simulations the Lennard-Jones potential is truncated at a particle separation of 3.5. In view of these differences and our introduction of the structureless fluid approximation, $g(s) = 1$, in the attractive energy part of the YBG equation, we feel the agreement betweeen the computer simulations and our predictions for the 6-$\infty$ Lennard-Jones fluid is quite good. Although we do not show the results here, comparison of density profiles at other porewidths were in similar agreement with computer simulations.

The predicted pore diffusivities as a function of porewidth are given in Fig. 2. The diffusivity approaches the bulk fluid value in an oscillatory manner for both the hard sphere and the 6-$\infty$ Lennard-Jones fluid, although the oscillations are sharper and persist to greater porewidths in the case of the Lennard-Jones fluid. Similar oscillations were observed in the molecular dynamics simulation of Magda *et*

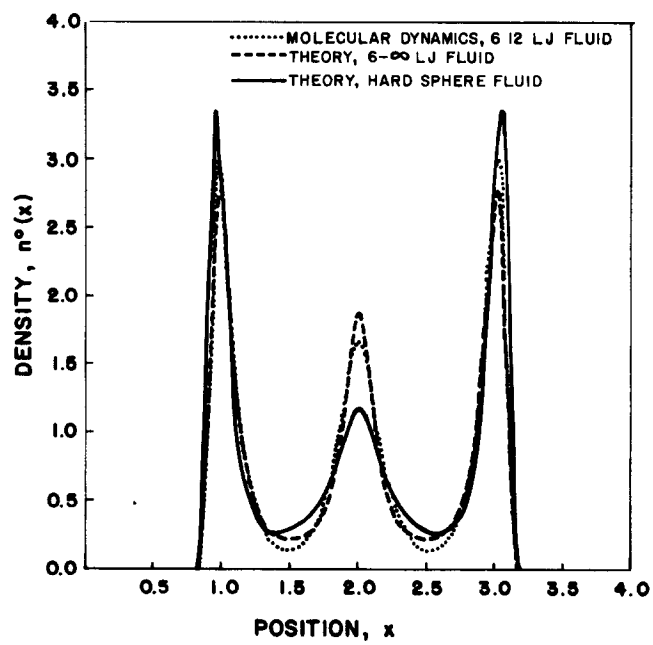


FIG. 1. Fluid density vs distance from pore wall. Computer simulations taken from Refs. 2 and 3.

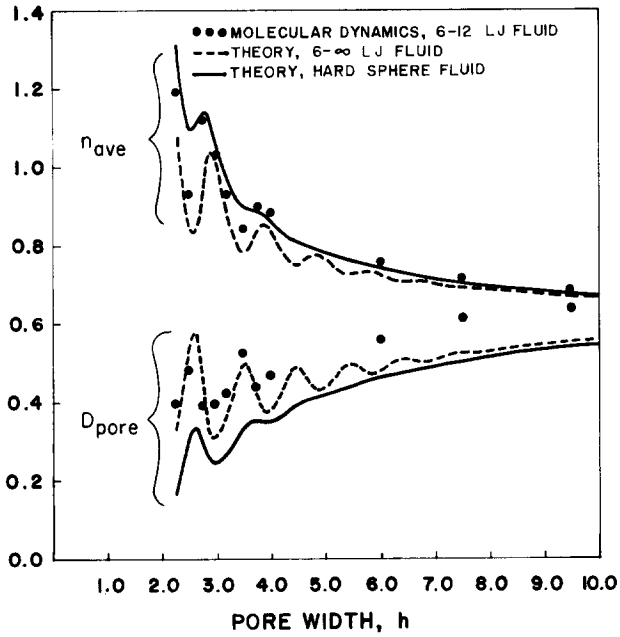


FIG. 2. Pore diffusivity and restricted pore average density vs porewidth. Computer results from Ref. 3.

*al.* Their results are also presented in Fig. 2. The local maxima and minima of the theoretical results and the simulations occur at nearly the same porewidths. The oscillations in the simulation results are not as sharp as those predicted for the 6-∞ Lennard-Jones fluid. We do not know whether this is the result of the difference between the fluid–fluid interaction potentials or a deficiency in the theory.

It has been found in bulk fluid correlations that hard sphere transport formulas give estimates of real fluid data (and computer data for Lennard-Jones fluids) if a temperature dependent effective hard sphere diameter is introduced.[7] We tried this approach by choosing an effective hard sphere diameter, $\sigma_{eff}$, so that the bulk hard sphere diffusivity agrees with the 6-12 LJ field at the same bulk density. The diameter was determined to be $\sigma_{eff} = 0.972$. The predicted pore diffusivities agree better with computer experiment (Fig. 3).

The oscillations in the pore diffusivity with porewidth result from layering of the fluid molecules between pore walls. When the wall separation favors a given integral number of layers, the average pore density attains a local maximum and the pore diffusivity correspondingly attains a local minimum. The density behavior is illustrated in Fig. 2, in which the restricted average pore density $n_{ave}$, defined by

$$n_{ave} = \frac{1}{h - 2\delta} \int_{\delta}^{h-\delta} n^0(x)dx$$

is plotted vs porewidth. $\delta$ is the thickness of the region near the pore wall which is empty of particles and therefore is not involved in the diffusion process. For the wall potential used in this work $\delta = 0.8$. Maxima and minima in $n_{ave}$ correspond to respective minima and maxima in $D_{pore}$. The predicted trends agree with those observed in the molecular dynamics simulations, also shown in Fig. 2. In the simulations the maxima and minima are shifted to slightly smaller porewidths, a trend consistent with the fact that the 6-12 Lennard-Jones potential is not infinitely repulsive at an interparticle separation of $\sigma$, whereas in our model the potential is infinitely repulsive at $\sigma$ (with the effective hard sphere diameter the maxima and the minima of the theory are in better agreement with the simulations as is apparent in the diffusivities given in Fig. 3).

At a porewidth of 2.95 two fluid layers are favored, $n_{ave}$ is a local maximum, and $D_{pore}$ is a local minimum. At a porewidth of 2.60 the two fluid layers are beginning to crowd into an unnatural packing and yet one fluid layer cannot fill the pore space (the porewidth at which one layer is favored is 1.95). Consequently, the two layers are defective, $n_{ave}$ is a local minimum, and $D_{pore}$ is a local maximum. The microscopic basis for this interpretation is shown in Figs. 4 and 5,

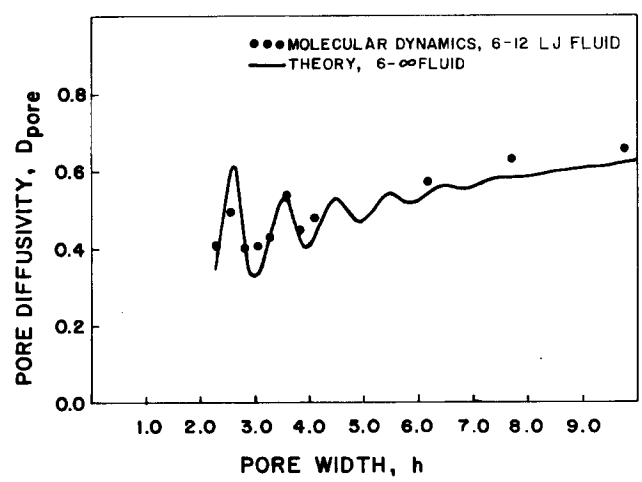


FIG. 3. Pore diffusivity vs porewidth. Theory is for 6-∞ LJ fluid with an effective hard sphere diameter of $\sigma_{eff} = 0.972\sigma$. Computer results from Ref. 3.

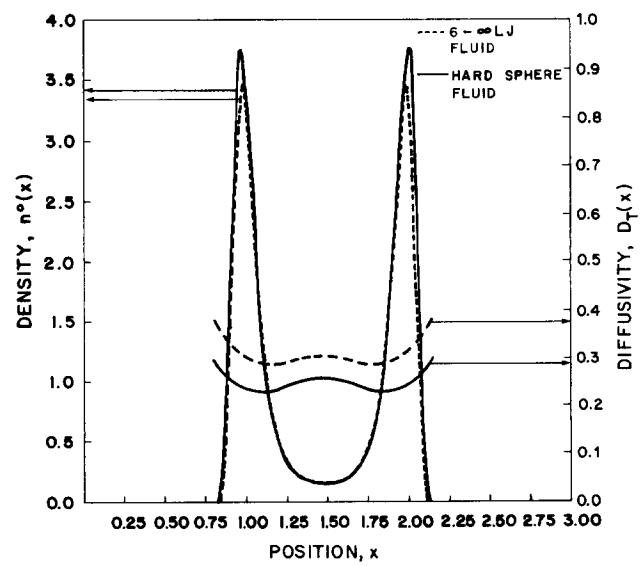


FIG. 4. Fluid density and local transverse diffusivity vs distance from pore wall in pore of width $2.95\sigma$.

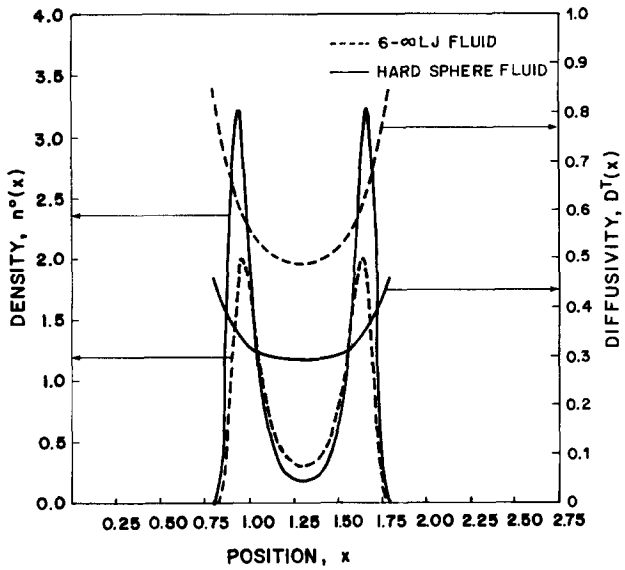


FIG. 5. Fluid density and local transverse diffusivity vs distance from pore wall in pore of width $2.60\sigma$.

in which $n(x)$ and $D_T$ are plotted vs position $x$ in pores of width 2.95 and 2.60, respectively. The peaks representing layered structures are sharper in the pore of width 2.95 than in the one of width 2.60 and the local diffusivity is correspondingly smaller.

A practical implication of this study is that the selectivity of microporous membranes, such as the zeolites, can be enhanced by exploitation of the porewidth dependence of the diffusivity of a molecule of a given size.

## ACKNOWLEDGMENTS

The authors are grateful to the ACS Petroleum Research Fund, the National Science Foundation, the Minnesota Supercomputer Institute for financial support of this research. We also would like to acknowledge the Graduate School of the University of Minnesota for the doctoral dissertation fellowship awarded to TKV.

[1] H. T. Davis, Chem. Phys. **86**, 1474 (1987).
[2] I. K. Snook and W. van Megen, Chem. Phys. **72**, 2907 (1980).
[3] J. J. Magda, M. V. Tirrell, and H. T. Davis, J. Chem. Phys. **83**, 1888 (1985).
[4] J. Fischer and M. Methfessel, Phys. Rev. A **22**, 2836 (1980).
[5] U. Heinbuch and J. Fischer (private communication, 1986).
[6] N. F. Carnahan and K. E. Starling, J. Chem. Phys. **51**, 635 (1969).
[7] J. H. Dymond and L. A. Woolf, J. Chem. Soc. Faraday Trans. **1**, 991 (1982).